SI: Vibrational Relaxation in EDTA Is Ion-Dependent

Sean C. Edington and Carlos R. Baiz*

Department of Chemistry, University of Texas at Austin, Austin, TX 78712

E-mail: cbaiz@cm.utexas.edu

S1. Transient absorption spectroscopy

Transient absorption measurements were taken using a custom-built 2D IR apparatus, which is illustrated schematically in Figure S1. The 800 nm, 100 fs, 12 μJ, 1 kHz repetition rate output of a Coherent Astrella Ti:sapphire regenerative amplifier was used to produce horizontally polarized mid-infrared pulses 100 fs in width and spectrally centered at 6.2 μm via optical parametric amplification in a Light Conversion TOPAS followed by difference frequency generation in a Light Conversion N-DFG. The mid-infrared pulses were split into excitation (95% of original pulse, transmitted), detection (2.5% of original pulse, reflected), and reference (2.5% of original pulse, reflected) beams using an uncoated CaF_2 wedge. Excitation pulses were modulated using a PhaseTech QuickShape Ge-based pulse shaper.[1,2] A two-frame phase cycle was used to remove residual scatter. The excitation and detection pulses were temporally overlapped by adjusting the optical path of the detection pulse with an Aerotech ANT95-L series linear nanopositioning stage. The reference pulse is not overlapped with the other two pulses and arrives at the sample area approximately 5 ns before the pump pulse pair. The polarization of the detection and reference pulses was controlled using a half-wave plate. The excitation, detection, and reference pulses were spatially overlapped in the sample using gold-coated parabolic mirrors. The detection and reference pulses were filtered by a wire grid polarizer (Optometrics) before being dispersed onto a Teledyne 128 pixel x 128 pixel IR camera with 40 μm pixel pitch by an Andor Shamrock spectrograph. The detection and reference pulses were aligned onto the IR camera such that the detection pulse fell on the upper 64 pixel rows and the reference pulse fell on the lower 64 pixel rows. Pixels in the reference and detection regions of the camera were vertically binned for a maximum bit depth of 20 bits. All spectrometer control and data collection was performed using software written in LabView. Data analysis and plotting were performed using MATLAB. All transient absorption data shown were collected in the perpendicular (ZZYY) polarization condition with the reference pulse blocked such that only the detection pulse fell on the IR camera. The path of the mid-infrared pulses was purged with -100° F dew point dry air such that no water vapor absorption features were visible in the detection spectrum. A total of 2000 laser shots were collected to produce each pump-probe spectrum.

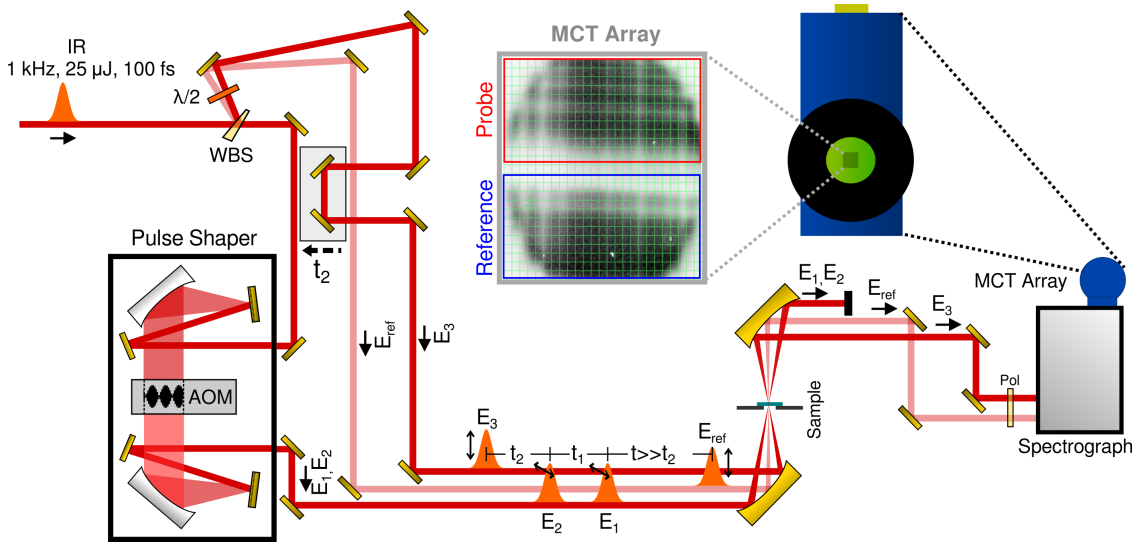

Figure S1: Schematic of 2D IR spectrometer used for pump-probe measurements. $\lambda/\mathbf{2}$, half-wave plate; **WBS**, wedge beam splitter; **AOM**, acousto-optic modulator; **MCT**, mercury cadmium telluride; $\mathbf{E_1}$, first excitation pulse; $\mathbf{E_2}$, second excitation pulse; $\mathbf{E_3}$, detection pulse; $\mathbf{E_{ref}}$, reference pulse; $\mathbf{t_2}$, excitation-detection delay. Direction of pulse propagation is denoted by single-headed arrows. Pulse polarization is denoted by double-headed arrows.

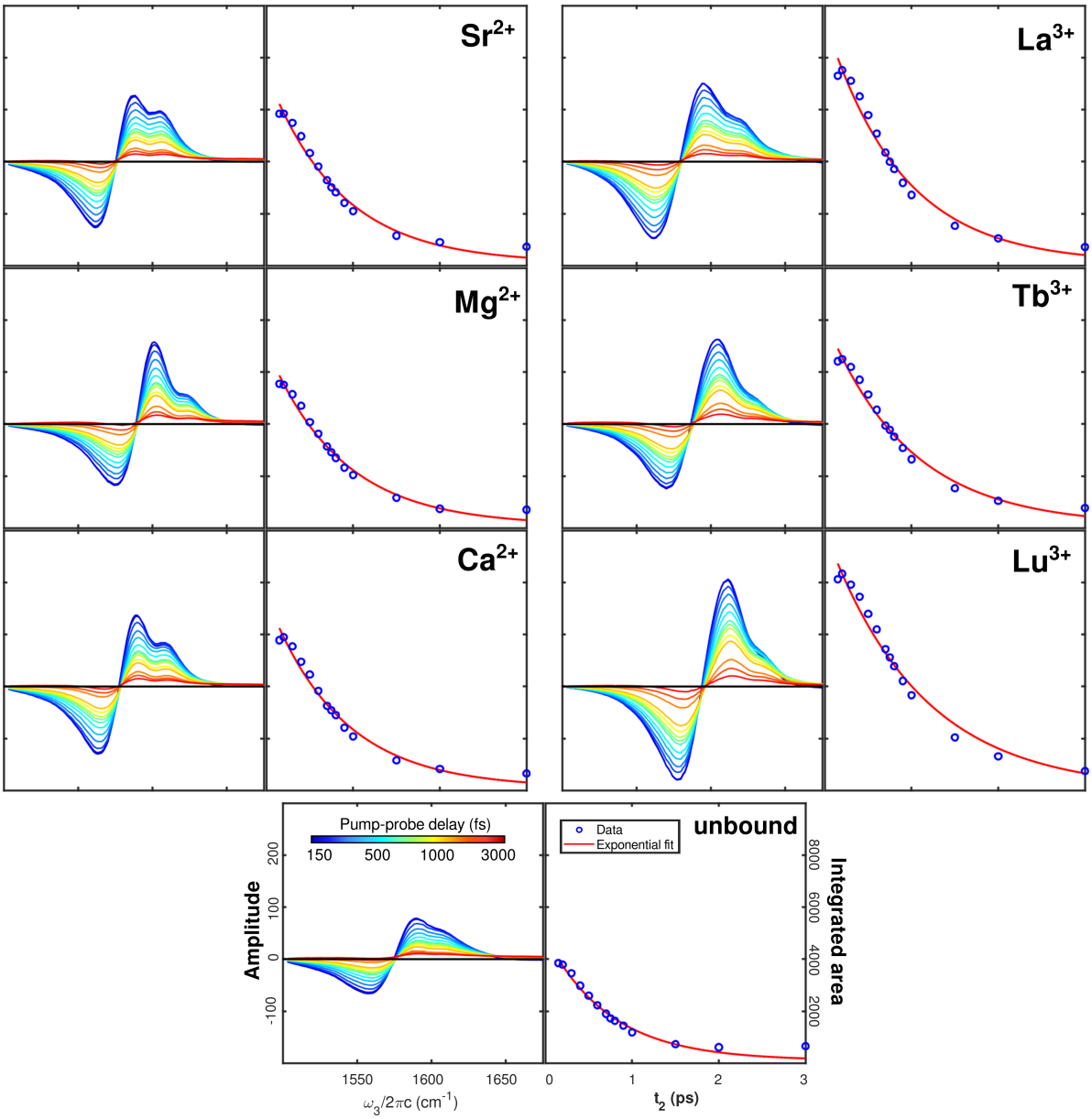

Figure S2: Typical series of transient absorption spectra and the corresponding single exponential fits. Amplitudes are extracted from the transient spectra by taking the integreated area of the transient absorption signal at each delay.

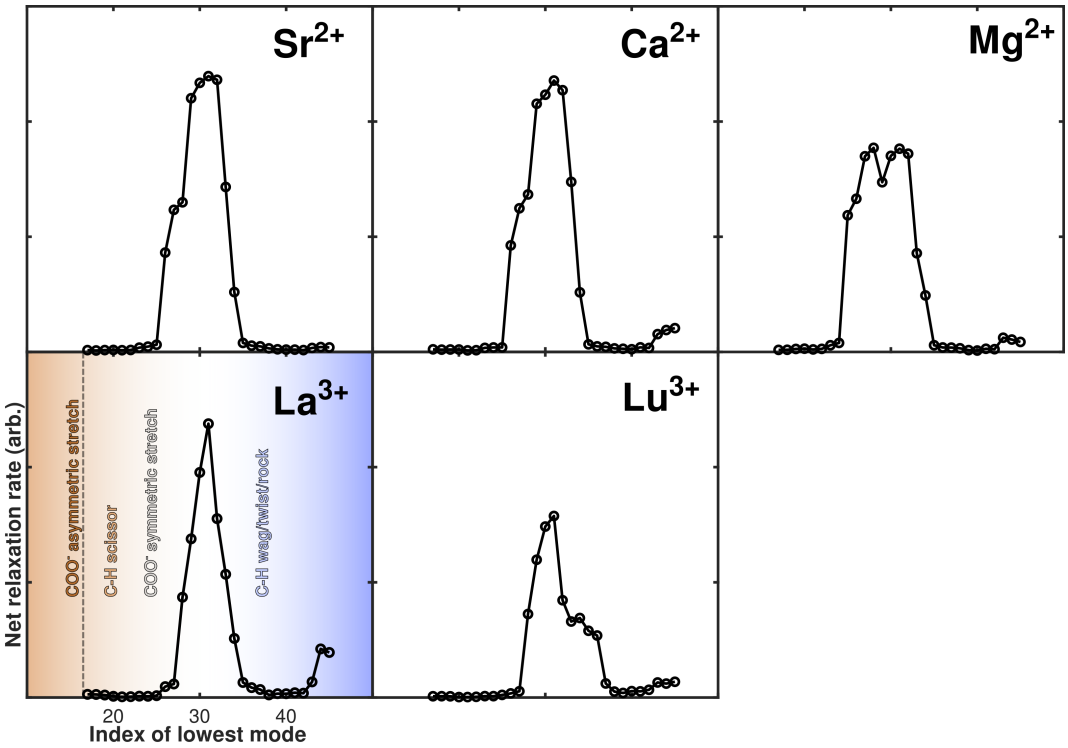

Figure S3: Comparison of vibrational relaxation rates from the four ν_a modes to different groups of lower-lying modes. EDTA has ninety-three normal vibrational modes; the ν_a modes are indexed 13, 14, 15, and 16 in order of decreasing energy in all EDTA complexes. We considered relaxation from the ν_a set 13-16 to all possible sets of four lower-lying contiguous normal modes through the 48th mode (17-20, 18-21, ..., 45-48). For each ion, traces were generated by scanning through all twenty-eight possible mode sets and plotting the calculated relative relaxation rate as a function of the lowest-indexed mode in the set. The traces show that practically all relaxation in EDTA complexes is captured using our choice of normal modes.

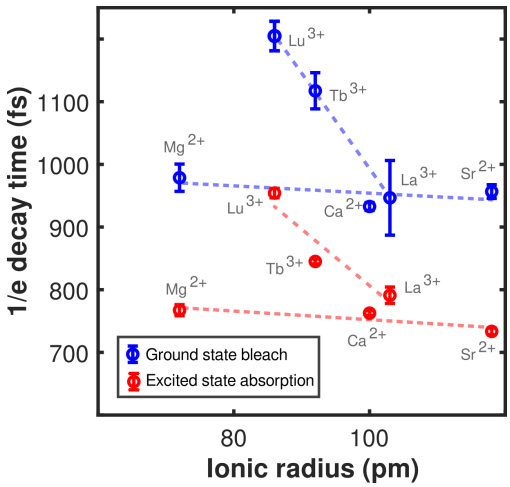

Figure S4: Time constants extracted from single exponential fits to ground state bleach and excited state absorption decays. As a supplement to analysis of the combined transient absorption signal, we analyzed the ground state bleach and excited state absorption signals separately. Amplitudes for the ground state bleaching signal and excited state absorption signal are extracted from the transient absorption spectra by taking the integrated area of the ground state bleach and excited state absorption at each delay. Time constants are derived by fitting the time series data to single exponential decays. Delay of the ground state bleach recovery relative to the excited state absorption is consistent with relaxation of the carboxylate asymmetric stretching modes through a manifold of lower-lying states.

S2. Vibrational relaxation model

To capture ion-dependent vibrational relaxation rates, we employ a Redfield-based approach based on the theory developed by Baiz and coworkers.[3,4] The methodology was originally developed to model coherence transfer and vibrational relaxation in metal carbonyls. Here, we simplify the Hamiltonian to capture energy redistribution rates within the carboxylate modes. More specifically, we compute the vibrational relaxation rates to capture ion-dependent trends in the vibrational lifetimes of the asymmetric carboxylate stretches. The computations are carried out in the normal-mode representation.

We start with a general system Hamiltonian of the form:

$$H_s = \sum_{j=0}^{n-1} (\hbar\omega_j) \, |1j\rangle\langle 1j| \tag{1}$$

Where $|1j\rangle$ represent the anharmonic vibrational states of the system consisting of the carboxylate modes. n is the total number of modes. In our case, there are total 8 modes for the system (4 carboxylate asymmetric stretching modes and 4 lower-lying modes, see main text). The first index indicates that these are singly-excited states, and the second index represents the states in order of increasing energy. In general, the system-bath coupling Hamiltonian is written in the basis of the system states as:

$$H_{BS} = \sum_{j=0}^{n-1} \sum_{k=0}^{n-1} |1j\rangle \hat{\Lambda}_{1j,1k} \langle 1k| \tag{2}$$

Where $\hat{\Lambda}$ represents the system-bath coupling operator, a bath operator that couples the system eigenstates. More specifically, we write the system-bath coupling Hamiltonian as a first-order expansion of the potential along the system eigenmodes:

$$H_{BS} = V\left(Q, 0\right) + \sum_{l=1}^{n} \left[\frac{\partial V}{\partial q_l}\right]_{q=0} q_l = V(Q, 0) + F_l\left(Q\right) q_l \tag{3}$$

Where q_l represents the coordinates of the l^{th} normal mode, F_l represents the force exerted by the bath onto the same mode, and Q are the bath coordinates such that:

$$\hat{\Lambda}_{1j,1k} = \sum_{l=1}^{n-1} q_{l;1j1j} F_l\left(Q\right) \tag{4}$$

Where $q_{l;1j1j} = \langle 1j|q_l|1j\rangle$. Note that these terms vanish for purely harmonic states. Finally, following the conventional Redfield approach, the energy transfer rates among the one-quantum states can be written in terms of the free bath force-force correlation functions as follows:

$$\Gamma_{ij,1m;1m,1j}(\omega) = \frac{1}{\hbar^2}\int_0^\infty d\tau e^{i\omega\tau}\left\langle \hat{\Lambda}_{1j,1m}(\tau)\hat{\Lambda}_{1m,1j}(0)\right\rangle \approx \frac{2}{\hbar^2}\sum_{l=1}^{n} q_{l;1j,1m}q_{l;1m,1j}\frac{\tilde{C}_{FF}(\omega)}{1+e^{-\beta\hbar\omega}} \tag{5}$$

Where we made the following approximation:

$$\tilde{C}_{FF}(\omega) = \int_0^\infty d\tau e^{i\omega\tau}\left\langle F_l(\tau)F_{l'}(0)\right\rangle \approx \mathrm{Re}\int_0^\infty d\tau e^{i\omega\tau}\left\langle F_l(\tau)F_{l'}(0)\right\rangle = \tfrac{1}{2}\int_{-\infty}^\infty d\tau e^{i\omega\tau}\left\langle F_l(\tau)F_{l'}(0)\right\rangle \tag{6}$$

And further:

$$\left\langle F_l(\tau)F_{l'}(0)\right\rangle = \delta\left(l,l'\right)\left\langle F_l(\tau)F_{l'}(0)\right\rangle \tag{7}$$

The first approximation is justified since the imaginary component of the Fourier transform represents a bath-induced frequency shift but does not affect the relaxation rates. [4]

The second approximation indicates that the forces along different normal modes are uncorrelated. This was previously found to be accurate for metal carbonyls. Finally, the relaxation rates constants can be written as:

$$k_{1m\leftarrow 1j} = 2\,\mathrm{Re}\left[\Gamma_{1j,1m;1m,1j}\left(\omega_{1j,1m}\right)\right] = \tfrac{4}{\hbar^2}\sum_{l=1}^{n}\frac{{q_{l;1j,1m}}^2}{1+e^{-\beta\hbar\omega_{1j,1m}}}\tilde{C}_{FF}\left(\omega\right) \tag{8}$$

In the case of ion-dependent relaxation rates, we assume that the force-force time correlation functions are the same for all ions. These correlation functions are typically computed using classical simulations. This can be justified since the force exerted by the solvent onto EDTA will be largely independent of the caged ion because the ion itself is not solvent-exposed. Furthermore, it is not currently possible to capture these interactions computationally since molecular dynamics force fields for lanthanides are not well-developed. Within this framework, any ion-dependent change in the relaxation rates is due to anharmonic coupling. We assume that relaxation of the asymmetric carboxylate modes proceeds primarily through the symmetric modes. These modes are separated by ca. 300 cm^{-1}, well within the spectral density of the bath.

Next, we describe the method for computing the anharmonic vibrational modes. To this end, we start with a general vibrational Hamiltonian of the form:

$$H = \sum_i \Phi_{ii}\left(p_i^2+q_i^2\right) + \sum_{i,j,k}\Phi_{ijk}\left(q_iq_jq_k\right) + \sum_{i,j,k,k}\Phi_{ijkk}\left(q_iq_jq_kq_k\right) \tag{9}$$

Where Φ_{ii}, Φ_{ijk}, and Φ_{ijkk} represent the mass-weighted second, third, and semi-diagonal fourth order

force constants.[5] These parameters are obtained by finite differentiation of the ground-state electronic potential along the mass-weighted normal mode coordinates using density functional theory.[6,7] More specifically, the harmonic Hessian is diagonalized at equilibrium and displaced geometries along each of the normal modes of interest, and the force constants are obtained as follows:

$$\Phi_{ijk} = \tfrac{1}{3}\frac{\Phi_{jk}(\delta q_i) - \Phi_{jk}(-\delta q_i)}{2\delta q_i} + \frac{\Phi_{ki}(\delta q_j) - \Phi_{ki}(-\delta q_j)}{2\delta q_j} + \frac{\Phi_{ij}(\delta q_k) - \Phi_{ij}(-\delta q_k)}{2\delta q_k} \tag{10}$$

$$\Phi_{ijkk} = \frac{\Phi_{ij}(\delta q_k) + \Phi_{ij}(-\delta q_k) - 2\Phi_{ij}(0)}{(\delta q_k)^2} \tag{11}$$

$$\Phi_{iikk} = \frac{\Phi_{ii}(\delta q_k) + \Phi_{ii}(-\delta q_k) - 2\Phi_{ii}(0)}{(\delta q_k)^2} + \frac{\Phi_{kk}(\delta q_i) + \Phi_{kk}(-\delta q_i) - 2\Phi_{kk}(0)}{(\delta q_i)^2} \tag{12}$$

Here the force constants Φ_{ij} are obtained by direct diagonalization of the Hessian matrix. The finite differentiation method has been used as implemented in the Gaussian 09 package of programs.

Once these force constants are computed, the Hamiltonian in equation 9, above is diagonalized to obtain the anharmonic modes.[8] The vibrational Hamiltonian is constructed in the basis of the normal modes, which includes eight C=O stretching modes (four symmetric and four asymmetric). The energy of the anharmonic states is converged with respect to the number of basis states. We have found that 5 basis states is sufficient to converge the energies. Once the anharmonic eigenstates are converged, the transition matrix elements of the form:

$$q_{l;1j,1m} = \langle 1j|\, q_l \,|1m\rangle \tag{13}$$

are simply computed using the anharmonic Hamiltonian in the same basis. Since these terms vanish in the Harmonic representation, accurate anharmonic states are important for extracting precise relaxation rates.

References

(1) Shim, S.-H.; Strasfeld, D. B.; Ling, Y. L.; Zanni, M. T. Automated 2D IR spectroscopy using a mid-IR pulse shaper and application of this technology to the human islet amyloid polypeptide. *Proc. Natl. Acad. Sci. U.S.A.* **2007**, *104*.

(2) Shim, S.-H.; Zanni, M. T. How to turn your pump-probe instrument into a multidimensional spectrometer: 2D IR and Vis spectroscopies via pulse shaping. *Phys. Chem. Chem. Phys.* **2009**, *11*, 748–761.

(3) Baiz, C. R.; Kubarych, K. J.; Geva, E. Molecular theory and simulation of coherence transfer in metal carbonyls and its signature on multidimensional infrared spectra. *J. Phys. Chem. B* **2011**, *115*, 5322–5339.

(4) Mulkamel, S. *Principles of Nonlinear Optical Spectroscopy*; Oxford University Press, 1999.

(5) Baiz, C. R.; Kubarych, K. J.; Geva, E.; Sibert III, E. L. Local-mode approach to modeling multidimensional infrared spectra of metal carbonyls. *J. Phys. Chem. A* **2011**, *115*, 5354–5363.

(6) Barone, V. Anharmonic vibrational properties by a fully automated second-order perturbative approach. *J. Chem. Phys.* **2005**, *122*, 014108.

(7) Dressler, S.; Thiel, W. Anharmonic force fields from density functional theory. *Chem. Phys. Lett.* **1997**, *273*, 71–78.

(8) Califano, S. *Vibrational States*; John Wiley & Sons, 1976.